Building Tomorrow's Society
Bâtir la Société de Demain

Fredericton, Canada
June 13 – June 16, 2018/ *Juin 13 – Juin 16, 2018*

NUMERICAL MODELLING OF DAPPED-ENDED GIRDERS REINFORCED WITH HEADED STUDS

Yuen, Kevin[1] and El-Badry, Mamdouh[1,2]
[1] University of Calgary, Canada
[2] melbadry@ucalgary.ca

Abstract: The use of headed studs as the primary shear reinforcement at the ends of dapped-ended girders has been proposed at the University of Calgary. Two analytical approaches – the shear friction and diagonal bending methods – were used to design the reinforcement layout of seven specimens, which were subsequently tested experimentally. Overall, results showed good agreement in failure loads between the experimental and analytical methods; however, several specimens exhibited greater error in one design method over the other when compared with the experiment. To provide further insight into the validity and accuracy of the shear friction and diagonal bending methods, a finite element analysis was conducted to further examine the performance of the tested specimens. A study consisting of four representative specimens showed that mesh size and the dilation angle parameter of the concrete damaged plasticity model had significant impacts on the accuracy of results. The latter appeared to be dependent upon the level of concrete confinement. Initial analyses yielded promising results and showed that the diagonal bending method is the more conservative approach; however, further refinements need to be applied to the current models.

1 INTRODUCTION

Dapped-ended girders have reduced cross sections at its ends such that the resulting "L" shaped profiles allow the member to rest on top of adjacent girders or support structures. Such members are particularly useful in bridges where it is often convenient to maintain continuity between girders of multiple spans, as well as providing allowance for expansion joints to be implemented. The 12.9 km-long Confederation Bridge, which connects Prince Edward Island with New Brunswick across the Northumberland Strait, uses dapped-ended girders for its hinged spans which were installed in a "drop-in" fashion. Due to the sudden reduction of cross sectional area of dapped girders, the corresponding effective depth available for shear resistance becomes reduced severely at the dapped ends. The re-entrant corners are vulnerable to diagonal shear cracking and ample reinforcement must be provided in these regions to allay such effects. An experimental program conducted by Herzinger and Elbadry (2007) showed that the use of headed studs can provide an effective alternative to conventional shear reinforcement. Comparatively speaking, its main advantages are the reduction of steel congestion around the re-entrant corner and improved anchorage properties due to bearing action from the heads.

2 SUMMARY OF EXPERIMENTAL PROGRAM

Seven specimens were investigated by Herzinger and Elbadry in their experimental study. The first two specimens, labelled DE-A-0.5 and DE-A-1.0, served as the controls and were reinforced conventionally at the dapped ends. A combination of vertical and horizontal studs served as the primary shear reinforcement in Specimens DE-B-0.5 and DE-B-1.0. Inclined studs were used in Specimen DE-C-1.0, while the final two specimens DE-D-1.0 and DE-D*-1.0 used a combination of horizontal, vertical, and inclined stud

configurations. The specimens were supported by an inclined roller-hinge assembly which induced horizontal reactions at the ends equal to twenty percent of the vertical reactions. Loading was performed using a spreader beam for the distribution of the two point loads. Measurements taken included the applied loads as a function of 45° displacement, and applied loads as a function of reinforcement strains at select locations.

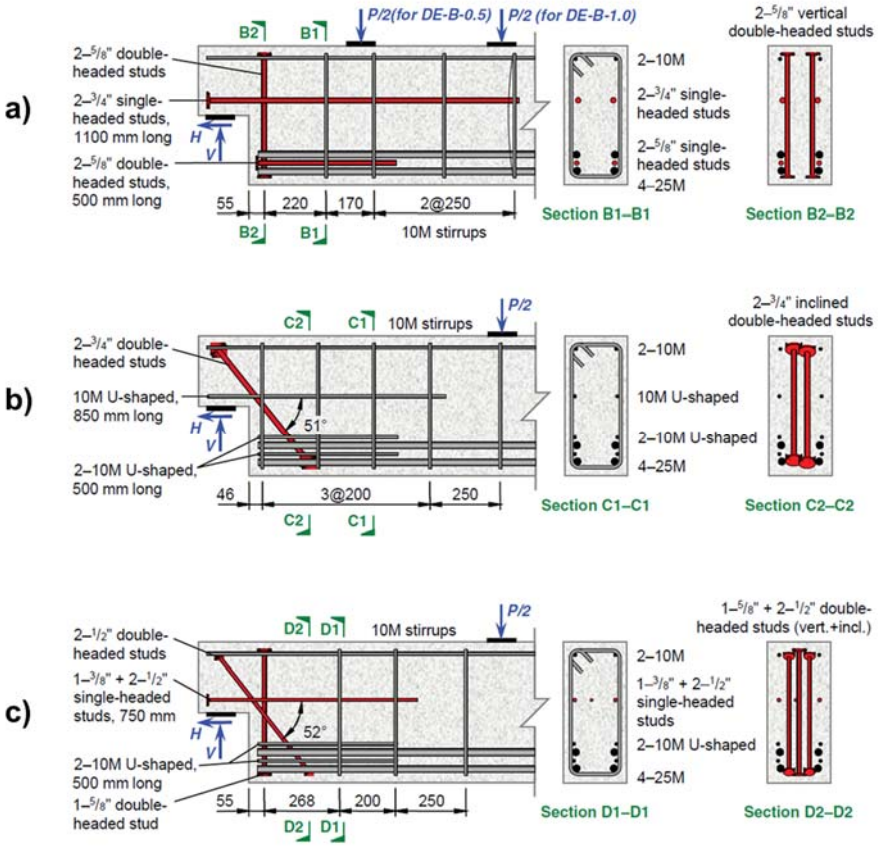

Figure 1: Details of specimens. a) DE-B-0.5/1.0, b) DE-C-1.0; and c) DE-D-1.0 *(Herzinger and Elbadry 2007)*

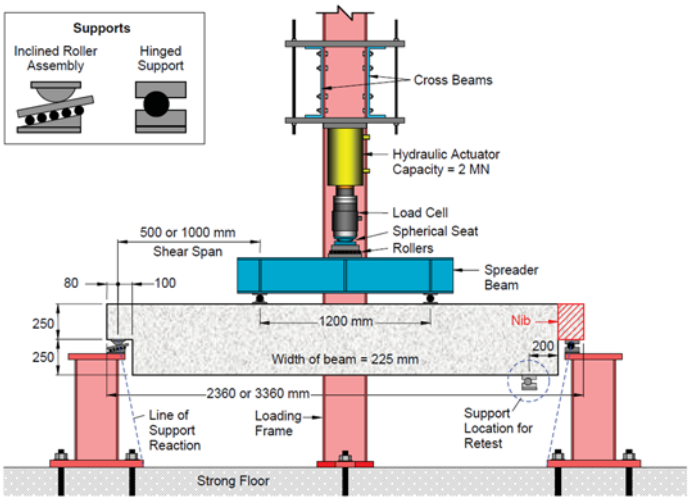

Figure 2: Experimental set up *(Herzinger and Elbadry 2007)*

3 NUMERICAL INVESTIGATION

3.1 Modelling Approach, Interactions, and Meshing

Four representative specimens were selected for the study: DE-B-0.5/1.0, DE-C-1.0, and DE-D-1.0. The finite element software ABAQUS was used to conduct the numerical study. The specimens were modelled as three dimensional components consisting of the concrete girder, reinforcing cage, hinge and roller support assemblies, and the spreader beam. Most components were modelled using solid 8-noded hexahedral elements with reduced integration (C3D8R). A mesh sensitivity analysis was performed using DE-B-0.5 as the representative specimen, with average concrete girder mesh sizes of 20, 10, and 7.5 mm being examined. All conventional reinforcement was meshed using B31 beam elements. For easier, less restrictive meshing, the concrete portion within the vicinity of the stud heads were treated as separate parts, and subsequently tied to the rest of the girder body. These areas were provided a finer mesh than that of the main girder to improve the quality of the tied interaction. Perfect bond was assumed between the concrete and all conventional reinforcement which consisted of deformed bars. Therefore, the embedded technique was used to constrain movement of the reinforcing cage (embedded element) from the girder body (host element). Double-headed studs had smooth stems which meant that cohesive interaction must be accounted for. Furthermore, bearing action of the heads is present in the headed studs; as a result, they were modelled as solid parts. Single headed studs passing through the re-entrant corner were also modelled as solid parts such that cohesive interaction could be reproduced. Significant shear failure was anticipated to occur near the re-entrant corners and hence it was assumed that the perfect bond assumption was not valid at these locations. The exceptions to the aforementioned were for the horizontal 5/8” single headed studs at the bottom of the full depth sections of DE-B-0.5/1.0, which was modelled similar to the conventional reinforcement since shear failure was not expected to occur at those locations.

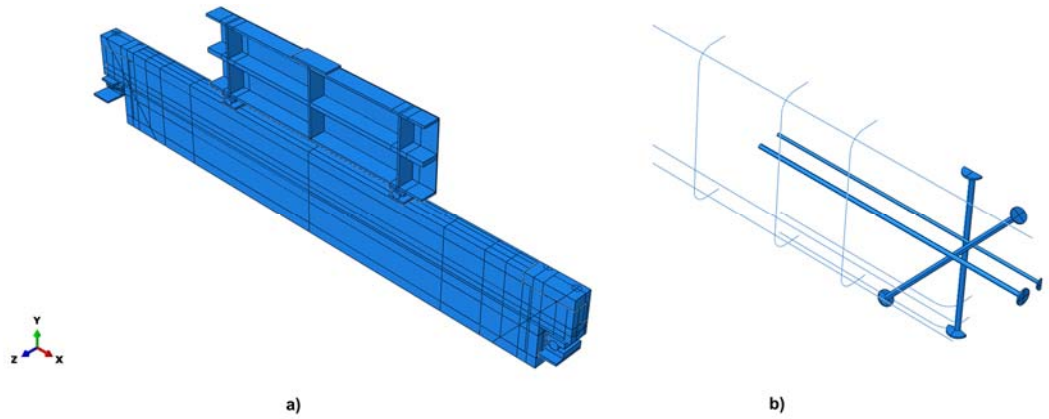

Figure 3: a) Typical model setup; and b) Typical reinforcing cage (detail at one end shown)

A stiffness-based cohesive interaction was specified between the headed stud stems and concrete. The maximum shear stress for which slipping will commence is taken as (CEB-FIP 2010)

[1] $\tau_{max} = 0.3(f'_c)^{1/2}$ for smooth bars; $\tau_{max} = 2.5(f'_c)^{1/2}$ for deformed bars

From the above, the tangential stiffnesses may therefore be expressed as (Henriques, da Silva and Valente 2012):

[2] $K_{ss} = K_{tt} = \tau_{max}/s_1$

where s_1, taken as 0.1 mm for smooth bars and 1.0 mm for deformed bars, is the interface slip (CEB-FIP 2010). No interface bond strength was assumed to exist in the normal direction. To specify damage in the cohesive interaction, a bilinear traction separation law was assumed. For simplicity, an arbitrarily large failure displacement of 1000 mm (Pereira 2015) was assumed to facilitate the plateau experienced in the

bond-slip between the stems and concrete after τ_{max} is reached. Since not more than several millimetres of slip were expected to occur, it was concluded that this assumption would be acceptable. Tie constraints were assigned between all bearing plates and the concrete girder. Steel-to-steel contact was specified between the surfaces of the roller support components as well as between the spreader beam supports and bearing plates. An exponential decay formulation was specified with coefficient of static friction μ_s = 0.74 and coefficient of kinetic friction μ_k = 0.57. Steel-to-concrete contact was specified between the stems and heads of the studs and concrete girder with μ_s = 0.60 and μ_k = 0.45. An arbitrarily large decay constant of 10^{10} was specified for simplicity for both steel-to-steel and steel-to-concrete contact. Lastly, the default "hard" normal contact was assumed in all cases as.

For all specimens, only half of their full size was modelled to exploit symmetry. Overlapping between the studs in Specimen DE-C-1.0 was ignored and the studs were shifted slightly such that they did not cross the plane of symmetry. As a consequence of symmetrical representation, the horizontal middle 3/8" studs in Specimen DE-D-1.0 were modelled as semi-circular solid components since a generalized beam profile could not be assigned inelastic material properties within the program.

3.2 Materials

3.2.1 Concrete

The concrete damaged plasticity model was used to represent the non-linear behaviour of concrete. The primary features of this model include a failure criterion, elastic-plastic strain decomposition, flow rule, work hardening rate equations which relate cohesion to the energy released in the non-linear portions of the compressive and tensile stress-strain curves (Lubliner, et al. 1989). The failure criterion is given as (Similia, 23.6.3 Concrete damaged plasticity 2013)

[3] $F = [1/(1 - \alpha)](q + 3\alpha p + \beta\langle\sigma_{max}\rangle - \gamma\langle\sigma_{max}\rangle) - \sigma_c$

with σ_{max}, p, and q being respectively the effective, hydrostatic, and Mises equivalent stresses. The parameters α, β, and γ are expressed as

[4] $\alpha = (f_{b0} - f_{c0})/(2f_{b0} - f_{c0})$; $\beta = (1 - \alpha)(\sigma_c/\sigma_t) - (1 + \alpha)$; $\gamma = 3(1 - K_c)/(2K_c - 1)$; $K_c = (J_{2,TM})^{1/2}/(J_{2,CM})^{1/2}$

where f_{b0} and f_{c0} are the initial equibiaxial and uniaxial compressive stresses, respectively, and f_{t0} is the initial uniaxial tensile yield stress. The compressive and tensile stresses σ_c and σ_t are the effective cohesive components. The parameter K_c is defined as the ratio of the square root of the second stress invariants between the tensile and compressive meridians (Lubliner, et al. 1989). A non-associated flow rule is used with the Drucker-Prager potential surface expressed as (Similia, 23.6.3 Concrete damaged plasticity 2013)

[5] $G = [(\epsilon\sigma_{t0}\tan\psi)^2 + q^2]^{1/2} - p\tan\psi$

where ψ is the dilation angle in the p-q plane at high confining pressures. The eccentricity parameter ϵ is set to a default value of 0.1. ABAQUS requires the input of five CDP parameters: ψ, f_{b0}/f_{c0}, ϵ, K_c, and a viscosity parameter μ. Due to lack of further data, default values of f_{b0}/f_{c0} = 1.16, K_c = 2/3, and μ = 0 were defined. The dilation angle ψ was varied in a sensitivity analysis using the representative specimen DE-B-0.5 for initial trial testing. The following compressive stress-strain model was adopted (Wahalathantri, et al. 2011):

[6] $\sigma_c = E_0\varepsilon_c$ for $0 \le \varepsilon_c < \varepsilon_{c@0.5f'c}$; $\sigma_c = f'_c[\beta(\varepsilon_c/\varepsilon_0)]/[\beta - 1 + (\varepsilon_c/\varepsilon_0)^\beta]$ for $\varepsilon_{c@0.5f'c} \le \varepsilon_c < \varepsilon_{c,end}$

where

[7] $\beta = 1/[1 - f'_c/(\varepsilon_0 E_0)]$; $\varepsilon_0 = 8.9 \times 10^{-5} f'_c + 2.114 \times 10^{-3}$ (f'_c in ksi); $E_0 = 124.3f'_c + 3283.12$ (f'_c in ksi)

Because a strain-based tensile model may introduce mesh sensitivity in regions with low reinforcement, a fracture energy-based model was instead employed (Similia, 23.6.3 Concrete damaged plasticity 2013). The following expression was adopted for the fracture energy G_F (CEB-FIP 2010)

[8] $G_F = 0.073(f_{cm})^{0.18}$ (in N/mm); $f_{cm} = f'_c + 8$ (in MPa)

Considering the following tensile stress-displacement curve (Hordijk 1992)

[9] $\sigma_t = f_{ctm}\{[1 + (c_1 w_t/w_{cr})^3]\exp(-c_2 w_t/w_{cr}) - (w_t/w_{cr})(1 + c_1^3)\exp(-c_2)\}$

the cracking displacement w_{cr} can be related to G_F through (Alfarah, Lopez-Almansa and Oller 2017)

[10] $w_{cr} = 5.14 G_F/f_{ctm}$

where f_{ctm} is the concrete tensile strength. The constants c_1 and c_2 were found to have values of 3 and 6.93 which best fit experimental data (Hordijk 1992). A simple damage model was incorporated in both the compressive and tensile regimes, which was expressed as the fraction of strength remaining following post peak response. Hence

[11] $d_i = 1 - \sigma_i/f_i$

where the subscript i denotes either tension or compression. In all specimens, Poisson's ratio v was taken as 0.2 while density was assigned a value of 2.4×10^{-9} tonne/mm^3. Compressive and tensile strengths were obtained from tests carried out prior to the experiments.

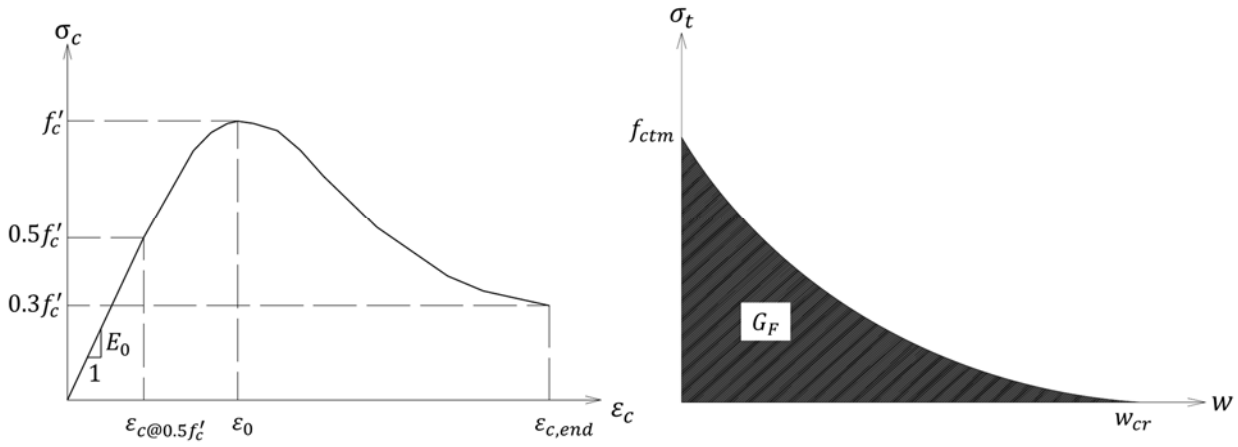

Figure 4: Uniaxial compression curve (left) and tensile-displacement curve (right)

3.2.2 Steel

A bilinear idealized stress-strain relationship was adopted for steel, whereby

[12] $f_s = E_s\varepsilon_s$, $\varepsilon_s < \varepsilon_y$; $f_s = f_y + [(f_u - f_y)/(\varepsilon_u - \varepsilon_y)]\varepsilon_s$, $\varepsilon_y \le \varepsilon_s < \varepsilon_u$

with the yield strain ε_y simply taken as f_y/E_s. The ultimate strain ε_u occurs at the end of the curve and was provided by curves developed through tensile tests performed before the experiment, along with yield and ultimate strengths and elastic moduli of all conventional reinforcement and headed studs. For all bearing components including plates, angles, supports, and the spreader beam, standard values of f_y = 400 MPa, f_u = 550 MPa, and E_s = 200 000 MPa were assumed. Poisson's ratio in all cases was taken as 0.3 while steel density was taken as 7.85×10^{-9} tonne/mm^3.

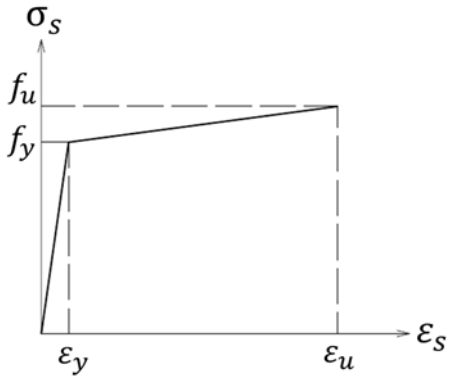

Figure 5: Adopted steel stress-strain curve

3.3 Solution Technique, Loads, and Boundary Conditions

Due to the highly inelastic behaviour of the model with multiple constraints and contact interactions, it was not possible to use the standard Newton's method to perform the analysis. Instead, a dynamic explicit scheme was employed and proper measures were taken to ensure quasi-static conditions. A time of 8 s was applied to the step duration with a mass scaling factor of 16 specified to artificially decrease computational time by roughly four fold. It was important to ensure that the values selected for these two parameters were such that inertial effects remained negligible. Gravity was applied to the entire model and varied in amplitude in a smooth step fashion from zero at the beginning of the step to its full value of 9810 mm/s^2 at t = 0.1 s, then held at full magnitude for the remainder of the analysis. An "empty" time period between 0.1-0.5 s was allocated to provide enough time for lingering movement or vibrations in the model to dissipate before load application started. In all models a specified displacement of 20 mm downwards with no movement in the longitudinal direction was specified for the bearing plate on top of the spreader beam. The amplitude of the displacement was defined using a smooth step curve, commencing at t = 0.5 s and ending at t = 8 s. The hinge and roller support bases were given encastre boundary conditions to entirely prevent their movement. Symmetry boundary conditions were applied to all the specimens about a plane bisecting the girder cross section longitudinally (normal in the z-direction). For Specimen DE-C-1.0, overlapping between the studs in the experimental setup was neglected; the studs were relocated a small amount to ensure that the model could be represented symmetrically.

4 RESULTS AND DISCUSSION

The load-45° displacement behaviour and failure patterns were the main results sought out in the analyses. As well, the strains in the headed studs of Specimen DE-D-1.0 were plotted as a function of applied load to verify member ductility. Based on the results, it was found that a finer mesh size led to more consistent results; as shown in Specimen DE-B-0.5 there was little difference between an average mesh size of 10 mm and 7.5 mm. In the 7.5 mm model, there was actuality localized excessive deformation in the second row of elements near the girder top at the hinged end of DE-B-0.5, which meant that when measuring the 45° displacement, one of the end nodes was required to be taken from the third, regularly deformed row of elements to maintain accuracy. An average mesh size of 10 mm was therefore adopted for the concrete girder in all other specimens. A sensitivity analysis showed that, for DE-B-0.5, the highest allowable dilation angle of 56.3° resulted in the most accurate behaviour in terms of maximum applied load and ductility. A maximum load of 425 kN was found for DE-B-0.5, differing from the experimental value by 5.7%.

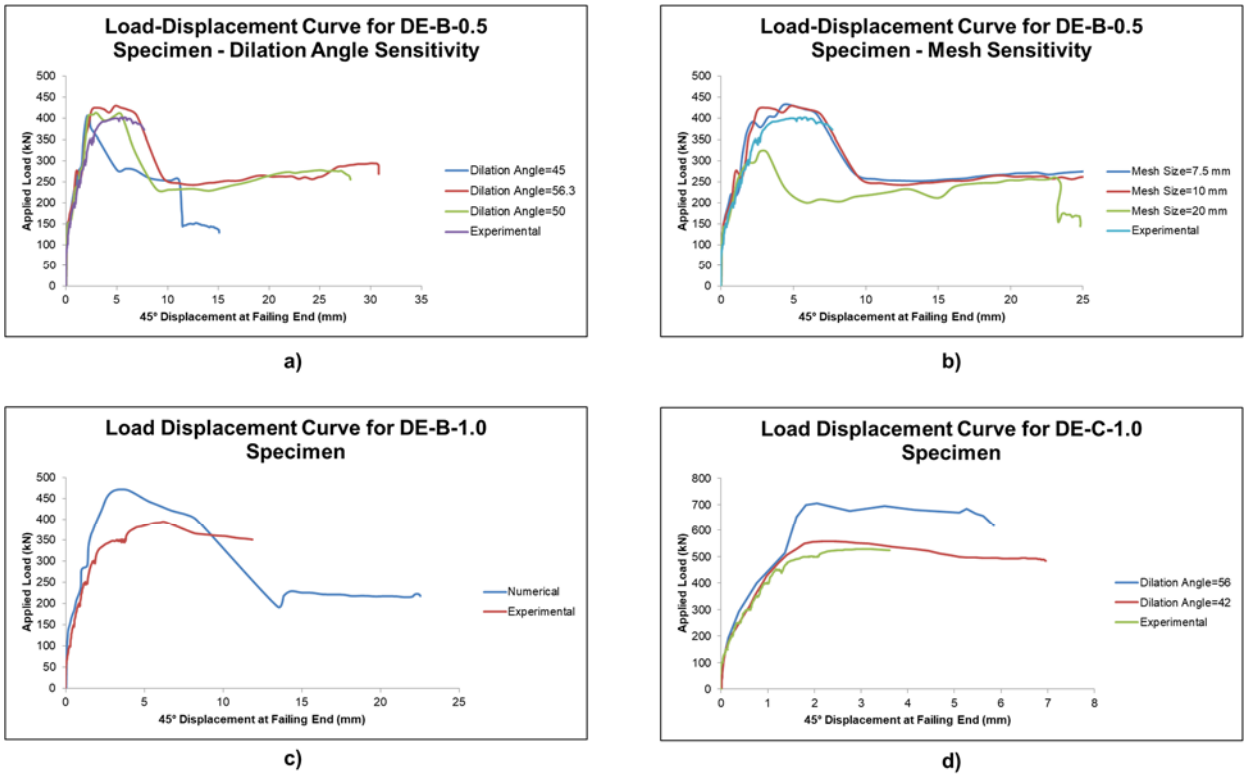

Figure 6: Load-Displacement curves at failing end for a) Specimen DE-B-0.5 (dilation angle analysis); b) DE-B-0.5 (mesh analysis); c) DE-B-1.0; and d) DE-C-1.0

A drop in applied load from the plateau occurred at roughly 7 mm displacement; there was a large gap between the two successive data points in the upper and lower plateaus which indicated that the specimen failed there. The same dilation angle value of 56.3° was adopted for Specimens DE-B-1.0, DE-C-1.0, and DE-D-1.0 to check its validity. The result for DE-B-1.0 was that the maximum load was almost twenty percent higher than in the experiment, albeit being slightly less ductile. Again, failure was taken as the point where there was a significant drop in applied load between the upper and lower plateaus with no intermediate data points, in this case at an approximate displacement of 8 mm.

Table 1: Summary of maximum loads of modelled specimens (kN)

Specimen	Numerical	Experimental	Shear Friction	Diagonal Bending
DE-B-0.5	425	402	407	441
DE-B-1.0	472	395	407	439
DE-C-1.0	557	528	622	496
DE-D-1.0	462	415	482	426

The lower plateau of Specimens DE-B-0.5/1.0 showed that some strength remained in the steel at the re-entrant corner; this behaviour was dependent on the dilation angle of the concrete as a result of the interaction between the two materials. Both DE-B-0.5/1.0 had similar failure patterns at the re-entrant corner and only one case is shown in Figure 8. As depicted in this figure, both DE-B-0.5/1.0 failed at the hinged support contrary to the experiment. From Figure 7, a maximum load of 462 kN was obtained for Specimen DE-D-1.0. Using the selected dilation angle of 56.3°, the maximum load was overestimated by 11.3% with respect to the experimental value. As well, while a plateau indicative of ductility was present, the descending branch obtained from the experiment was not captured. The maximum displacement for DE-D-1.0 of 7.6

mm was limited to the displacement boundary condition specified and was cut off due to completion of the analysis. For this reason, the failure pattern at peak load and end of analysis were identical, as shown in Figure *8*. The hinged end was taken as the location where failure would occur first; the vertical and inclined stud strains not only demonstrated this, but provided verification of member ductility by showing significant yielding. The average horizontal stud strains in the west end, however, yielded far more than those at the east end.

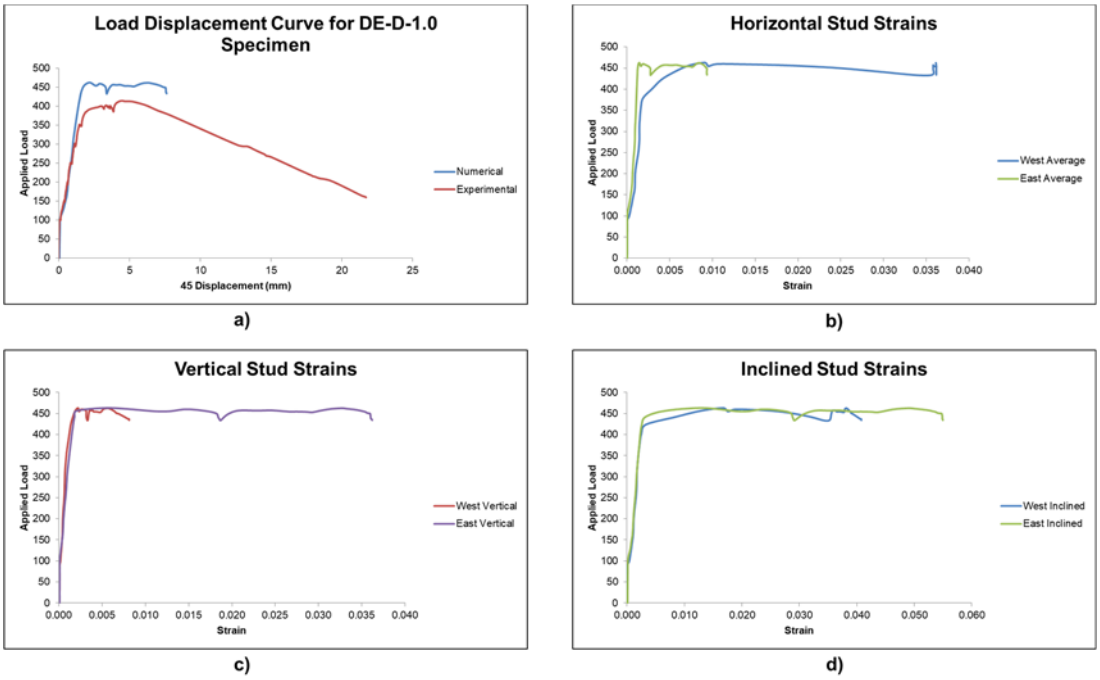

Figure 7: Load-displacement curve for **a)** DE-D-1.0 Specimen at failing end **b)** DE-D-1.0 average horizontal stud strains **c)** DE-D-1.0 vertical stud strains; and **d)** inclined stud strains

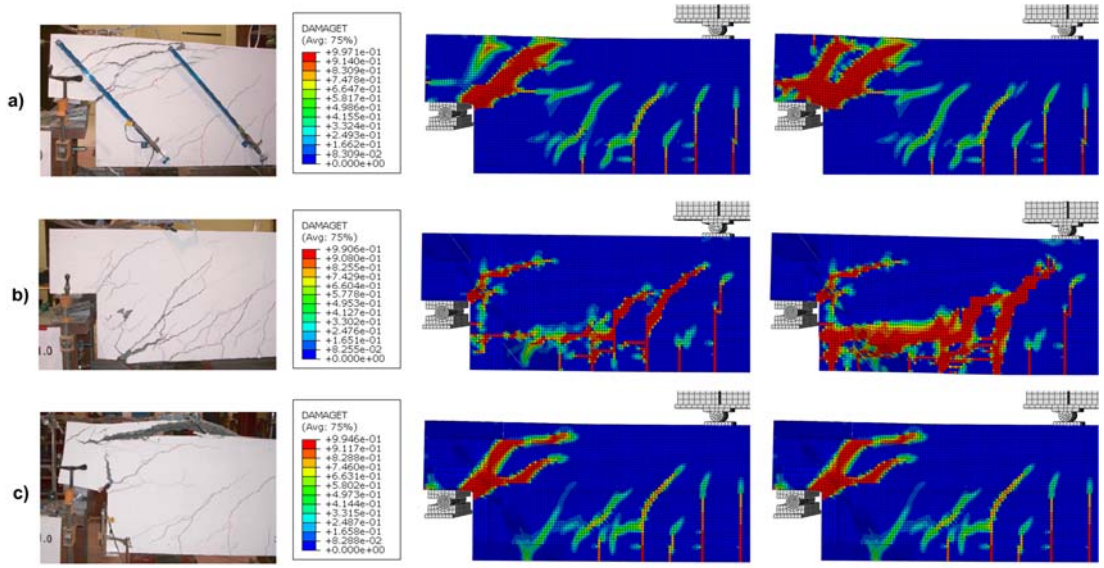

Figure 8: Experimental *(Herzinger and Elbadry 2007)* and numerical failure patterns: **a)** DE-B-0.5/1.0 immediately before (left) and after (right) failure; **b)** DE-C-1.0 at peak load (left) and analysis end (right); and **c)** DE-D-1.0 at peak load (left) and analysis end (right)

For Specimen DE-C-1.0, it was found that, when compared with the other three models, using the selected dilation angle value of 56.3° yielded in an excessive failure load of nearly 700 kN and greater ductility than in the experiment. This may be explained by the presence of stirrups at the re-entrant corner of the girder which provided some level of confinement to the concrete. It was observed that there was less bulging at the re-entrant corners, indicating that confinement may be present. A high dilation angle yielded relatively more accurate behaviour for the specimens where stirrups were not present at the re-entrant corner. It is suggested that for concrete with low levels of confinement, a higher range of dilation angle values may be assigned (Malm 2009). Hence, a lower dilation angle of 42° was chosen and resulted in a maximum load of 557 kN. As before, the specimen remained more ductile than in the experiment and did not fail at any point during the analysis. Smaller values of dilation angles, such as 40° and 35°, were attempted but led to premature errors in the analysis which led to their termination. It was found that several elements in the concrete girder distorted excessively, which is likely indicative of problems with the contact interaction between the concrete and studs. From Figure 8, in the numerical model the majority of the failure occurred in the full-depth portion of the girder surrounding the lower area of the diagonal stud, which agrees with the experimental result as failure was directed away from the re-entrant corner.

An important check for quasi-static loading conditions was made comparing the ratio of internal energy to kinetic energy of the whole model. In all cases, internal energy remained well below five percent of kinetic energy, which is the suggested limit for quasi-static conditions

5 CONCLUSIONS AND FUTURE WORK

In summary, four specimens from the experiments of Herzinger and Elbadry were selected in this study and analyzed numerically for their behaviour. While preliminary studies suggest promising correlation between the finite element models and experimental results, as a whole, further studies need to be performed, in part to examine the effect of the dilation angle parameter on model behaviour. As well, the applied displacements should be increased for specimens where relatively high ductility is expected. The final specimen DE-D*-1.0 will be analyzed next for further confirmation of the modelling approach undertaken. Coupled with the existing experimental work, data from the numerical study further suggest that the diagonal bending method of analysis provides the most conservative design approach. Specimen DE-B-1.0 is an outlier thus far as experimental and numerical results conflict. Upon confirmation of model validity, future parametric studies can be performed, making it possible to design dapped-ended girders reinforced with headed studs using other combinations of geometry and reinforcement layout.

Acknowledgements

This research was financially supported by the Natural Sciences and Engineering Research Council of Canada (NSERC) which is gratefully acknowledged.

References

Alfarah, B., Lopez-Almansa, F., and Oller, S., "New methodology for calculating damage variables evolution in Plastic Damage Model for RC Structures." *Engineering Structures*, 2017: 1-31.

CEB-FIP. "Model Code 2010 - First Complete Draft." Lausanne, Switzerland: Federation Internationale du beton, 2010.

Henriques, J., L.S. da Silva, and I.B. Valente. "Numerical modeling of composite beam to reinforced concrete wall joints - Part I: Calibration of joint components." *Engineering Structures* 52 (2012): 747-761.

Herzinger, R, and M Elbadry. "Alternative Reinforcing Details in Dapped Ends of Precast Concrete Bridge Girders." *Journal of the Transportation Research Board*, 2007: 111-121.

Hordijk, D.A. "Tensile and Tensile Fatigue Behaviour of Concrete; Experiments, Modelling and Analysis." *Heron* 37, no. 1 (1992): 1-77.

Lubliner, J., J. Oliver, S. Oller, and E. Onate. "A Plastic-Damage Model for Concrete." *International Journal of Solids and Structures* 25, no. 3 (1989): 299-326.

Malm, R. *Predicting shear type crack initiation and growth in concrete with non-linear finite element method.* Thesis, Stockholm: Royal Institute of Technology, Department of Civil and Architectural Engineering, Division of Structural Design and Bridges, 2009.

Pereira, H., Cunha, V, Sena-Cruz, J. "Numerical simulation of galvanized rebars pullout." *Frattura ed Integrita Strutturale*, 2015: 54-66.

Similia. *2.2.25 Concrete Damaged Plasticity, ABAQUS Verification Guide.* Providence, RI: Dassault Systemes Similia Corp., 2013.

Similia. *23.6.3 Concrete damaged plasticity.* Providence, RI: Dassault Systemes Similia Corp., 2013.

Similia. *28.1.1 Solid continuum elements, ABAQUS Analysis User's Manual.* Providence, RI: Dassault Systemes Similia Corp., 2013.

Wahalathantri, B.L., C.P. Thambiratnam, T.H.T. Chan, and S. Fawzia. "A material model for flexural crack simulation in reinforced cocnrete elements using ABAQUS." *Proceedings of the First International Conference on Engineering, Designing and Developing the Built Environment for Sustainable Wellbeing.* Brisbane, Queensland, 2011.